Spin reorientation and large magnetic anisotropy of metastable bcc Co islands on Au(001)

T. Miyamachi,[1,2,*] T. Kawagoe,[3] S. Imada,[1,4] M. Tsunekawa,[1,5] H. Fujiwara,[1] M. Geshi,[6] A. Sekiyama,[1] K. Fukumoto,[7,8] F. H. Chang,[9] H. J. Lin,[9] F. Kronast,[10] H. Dürr,[10,11] C. T. Chen,[9] and S. Suga[1,12,13]

[1]*Graduate School of Engineering Science, Osaka University, Toyonaka, Osaka 560-8531, Japan*
[2]*Institute of Solid State Physics, The University of Tokyo, 5-1-5 Kashiwanoha, Kashiwashi, Chiba 277-8581, Japan*
[3]*Division of Natural Science, Osaka Kyoiku University, Kashiwara, Osaka 582-8582, Japan*
[4]*Department of Physical Sciences, Ritsumeikan University, Kusatsu, Shiga 525-8577, Japan*
[5]*Faculty of Education, Shiga University, Otsu 520-0862, Japan*
[6]*Institute for Nanoscience Design, Osaka University, Toyonaka, Osaka 560-8531, Japan*
[7]*Japan Synchrotron Radiation Research Institute, Mikazuki, Sayo, Hyogo 679-5198, Japan*
[8]*Tokyo Institute of Technology, Meguro-ku, Tokyo 152-8550, Japan*
[9]*National Synchrotron Radiation Research Center, 101 Hsin-Ann Road, Hsinchu 30076, Taiwan*
[10]*Helmholtz Zentrum Berlin für Materialien und Energie, BESSY II, Albert-Einstein Straße 15, Berlin 12489, Germany*
[11]*Stanford Institute for Materials and Energy Sciences, SLAC National Accelerator Laboratory, Menlo Park, California 94025, USA*
[12]*Institute of Scientific and Industrial Research, Osaka University, 8-1 Mihogaoka, Ibaraki, Osaka 567-0047, Japan*
[13]*Max-Planck Institute for Microstructure Physics, Weinberg 2, Halle 06120, Germany*

(Received 15 February 2012; published 11 November 2014)

We studied magnetism and morphology of metastable bcc Co nanostructures on Au(001) by x-ray magnetic circular dichroism in combination with scanning tunneling microscopy and photoelectron emission microscopy. While room-temperature deposition of Co onto Au(001) leads to the formation of bcc Co thin films with pure in-plane magnetization, postannealing of these thin films at 500 K drastically changes the morphology to bcc Co islands embedded in Au. In accordance with this morphological change, we find that an out-of-plane magnetization emerges additionally and the coexistence of in-plane and out-of-plane remanent magnetizations is observed for the islands. The nanostructure-size dependence of magnetic moments suggests that the magnetization easy axis of the island changes from the in-plane to the out-of-plane direction with decreasing nanostructure size. Such a spin reorientation transition is likely due to the increased fractional population of rim atoms generating the out-of-plane magnetization in the smaller islands. The observed out-of-plane remanent magnetization of the smaller islands indicates their large magnetic anisotropy.

DOI: 10.1103/PhysRevB.90.174410 PACS number(s): 75.50.−y, 75.70.−i, 68.37.−d

I. INTRODUCTION

The final goal of miniaturization for information storage is to realize extremely small magnetic bits operating at room temperature. For this purpose, tiny bits must overcome thermal fluctuations. The thermal stability of bits relies on a magnetic anisotropy energy (MAE). Recent experimental and theoretical advances in nanoscale magnetic systems have revealed several key concepts to induce the giant MAE to nanostructures, i.e., (1) lowering the coordination number of atoms [1], (2) the interfacial effect with surroundings [2], and (3) electronic band structures [3]. So far, concept 1 was mainly emphasized to enhance the MAE of magnetic atoms. As the atomic coordination is reduced from bulky materials to thin films and further to two-dimensional (2D) nanostructures, the orbital magnetic moment is enhanced, resulting in the giant MAE per atom [1,4] since the MAE and orbital magnetic moment are strongly linked via spin-orbit (SO) interaction [5]. Within 2D nanostructures, larger magnetic moments and MAE of rim atoms owing to the lower symmetry are also reported [6–8]. On the other hand, the reduction of volume leads to weaker ferromagnetic coupling energy in finite-sized 2D nanostructures, inducing the superparamagnetic behavior [9] at higher temperatures of practical interest. One possible approach to enhance the MAE of finite-sized 2D nanostructures is to fabricate pseudo-three-dimensional (3D) nanostructures by vertically stacking atoms while keeping the lateral size. In such nanostructures, the MAE could be enhanced compared to simple 2D nanostructures with the same lateral size due to the increased volume. Despite the merit of vertical stacking, the technological difficulty remains to stack a sufficient number of atoms to be ferromagnetic at room temperature while keeping the lateral size. Hence, incorporation of concepts 2 and 3 in the vertical stacking is one of the promising directions toward practical nanostructure fabrication.

To fulfill these conditions, we artificially grew pseudo-3D bcc Co islands embedded in Au in this study. In addition to the vertical stacking, the interfacial effect with surrounding Au atoms and characteristic electronic band structures of the metastable bcc Co phase could enhance the MAE of the islands further than simple lowering of the atomic coordination, resulting in room-temperature ferromagnetism. The experimental results suggest that the coexistence of in-plane and out-of-plane remanent magnetizations observed for the islands derives from the nanostructure-size driven spin reorientation transition (SRT) of the magnetic easy axis; i.e., relatively larger islands favor the in-plane magnetization, while smaller ones are likely to be magnetized out of plane.

II. EXPERIMENTAL DETAILS

A reconstructed Au(001) surface was first grown on a 3-nm-thick Cr precovered MgO(001) [10]. All samples in this

*toshio.miyamachi@issp.u-tokyo.ac.jp

study were prepared by molecular beam epitaxy (MBE) from a high-purity Co rod (99.998%) onto this Au(001) surface. The base pressure of the MBE chamber was below 5×10^{-11} Torr. Since highly characterized samples are needed to investigate the relationship between magnetism and morphology, their morphology was first accurately determined by scanning tunneling microscopy (STM) in a constant-current mode at room temperature. Samples were then capped with 2-nm-thick Au *in situ* before transportation through the atmosphere to chambers for magnetic measurements. Such capping prevents oxidation in atmospheric conditions while allowing the detection of magnetic signals.

Magnetic moments of the samples were investigated by x-ray magnetic circular dichroism (XMCD). The measurements were performed at Dragon beamline BL11A of National Synchrotron Radiation Research Center in Taiwan by the total-electron-yield method at room temperature. The energy resolution $E/\Delta E$ was better than 10 000 and the circular polarization of the incident x ray was 83%. In the XMCD measurements, the circular polarization of the x ray was fixed and the direction of the applied magnetic field up to 1 T was reversed. The magnetization directions of magnetic domains at remanence were determined by a photoelectron emission microscope combined with XMCD (XMCD-PEEM) at room temperature. Measurements were performed at UE49-PGMa of BESSY in Germany. The incident circular x ray was nearly full polarized. XMCD and XMCD-PEEM measurements were well reproduced at BL25SU [11] of SPring-8 in Japan.

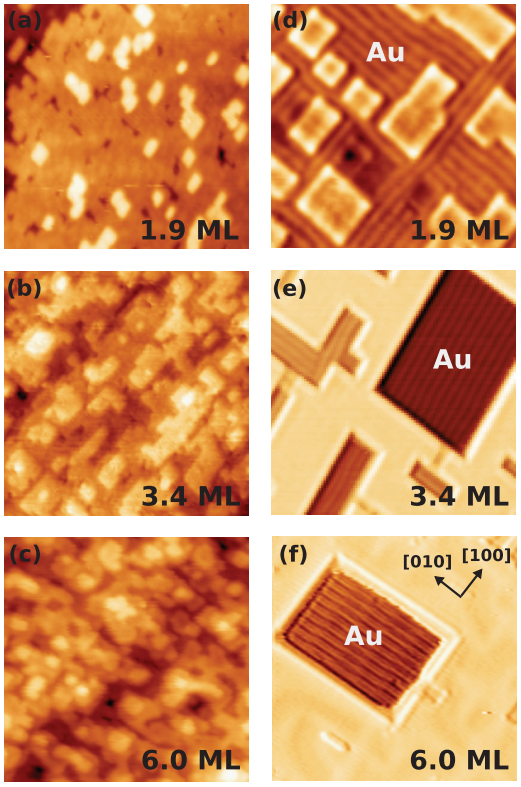

FIG. 1. (Color online) STM images of (a) 1.9 ML, (b) 3.4 ML, and (c) 6.0 ML bcc Co thin films (RT) and (d) 1.9 ML, (e) 3.4 ML, and (f) 6.0 ML bcc Co nanostructures (PA) on Au(001). The size of each image is 24×24 nm^2.

III. RESULTS AND DISCUSSION

A. Morphology

To fabricate bcc Co nanostructures, we first grew bcc Co thin films by room-temperature deposition of Co onto Au(001) (these samples are hereafter called RT). Figure 1(a) shows the STM image of 1.9 monolayer (ML) Co on Au(001) grown at room temperature (hereafter expressed as 1.9 ML RT). Its morphology is composed of the film surface with small islands. From the characteristic 1 ML height difference of about 0.14 nm and $p(1 \times 1)$ low-energy electron-diffraction (LEED) pattern with a lattice constant of about 0.28 nm, it is found that deposited Co is epitaxially grown on Au(001) with the bcc phase [12]. As the coverage is increased up to 3.4 and 6.0 ML as shown in Figs. 1(b) and 1(c), the island growth is promoted, resulting in rough surfaces. However, we also confirm from height profiles and LEED patterns that the bcc structure is still sustained at these coverages.

Pseudo-3D bcc Co islands are fabricated by postannealing of these bcc Co thin films (RT) at 500 K (these samples are hereafter called PA). The surface of PA prepared from 1.9 ML RT (expressed as 1.9 ML PA) is composed of the reconstructed Au(001) surface and rectangular islands as shown in Fig. 1(d). Gaussian fitting of the size distribution of 363 islands in the whole measured region in Fig. 2(a) leads to a mean lateral dimension of 3.8 nm with a full width at half maximum of 1.8 nm. The morphology of the islands was determined by STM to be 4 (5) ML bcc Co with a 2 (1) ML Au surfactant layer in the rim (core) region as shown in Fig. 2(b) (details are given in [10]). The rim width of about 0.5 nm corresponds to four atoms numbered as 1–4. The slight difference of height between the rim and core regions (0.06 nm) shown in Fig. 2(c) is definitely caused by 1 ML height difference between Au(001) and bcc Co (001) (Au, 0.20 nm; bcc Co, 0.14 nm). The origin of the pseudo-3D bcc Co islands embedded in Au would be due to the immiscibility of these two metals and large difference in their surface free energies [13]. In this study, three nanostructures with different morphology were prepared by changing the Co coverage. The morphology starts to change from isolated islands in 1.9 ML PA to network structures in 3.4 ML PA [Fig. 1(e)] due to the coalescence of islands. In 6.0 ML PA, the coalescence is further promoted, resulting in a considerably reduced fraction of the rim [Fig. 1(f)].

B. Magnetic moments

The magnetism of PA is studied and compared to that of RT by using XMCD. XMCD spectra are obtained in the total-electron-yield mode at room temperature by detecting $I_+ - I_-$, where I_+ and I_- denote the x-ray-absorption spectra (XAS) with the photon spin parallel and antiparallel to the majority-spin direction. The photon incidence angle is deviated by 30° from the direction of **B**. A magnetic field **B** of 1 T was applied either parallel ($\mathbf{B}_\parallel$) or perpendicular ($\mathbf{B}_\perp$) to the sample surface. Thus, the spectra for $\mathbf{B}_\parallel$ and $\mathbf{B}_\perp$ are sensitive to the in-plane and out-of-plane magnetizations of samples. Figure 3(a) shows XAS and XMCD spectra of 3.4 ML RT at the Co $L_{2,3}$ absorption edges. An XMCD signal

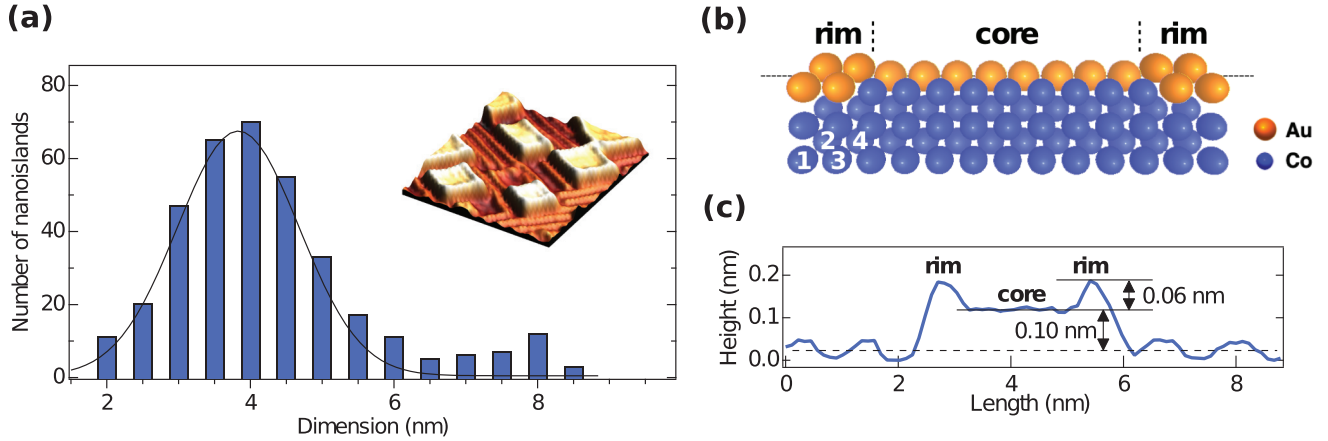

FIG. 2. (Color online) (a) Size distribution of bcc Co islands. Lateral dimension is given by substituting each island by a square with the same area. (b) Schematic cross-sectional view of a bcc Co island. Orange and blue spheres represent Au and Co atoms. Numbers show the column number of the Co atom in the rim. Outside the rim, Au atoms are piled up to the level shown by the dashed horizontal line. (c) Height profile of a typical bcc Co island (1.9 ML PA). The dashed horizontal line is set to zero.

is only observed for the $\mathbf{B}_{\parallel}$. The absence of the out-of-plane magnetization and a strong in-plane XMCD are consistent with previous results [14], reflecting the strong in-plane anisotropy of bcc Co thin films [15,16]. The in-plane magnetization might show up in the XMCD spectrum recorded in the $\mathbf{B}_{\perp}$ geometry in our XMCD alignment. Nevertheless, note that the $\mathbf{B}_{\perp}$ XMCD signal is not seen for 1.9 and 6.0 ML RT. This is because the in-plane magnetization of all the samples is averaged out by the demagnetization process just before the $\mathbf{B}_{\perp}$ XMCD measurements. Thus, we emphasize in this study that the out-of-plane magnetization and the in-plane magnetization are disentangled in the $\mathbf{B}_{\perp}$ geometry, and $\mathbf{B}_{\perp}$ XMCD signals are only attributable to the out-of-plane magnetization of the sample.

If PA has similar magnetic properties as RT, no $\mathbf{B}_{\perp}$ XMCD is expected. However, in addition to the in-plane magnetization, 3.4 ML PA definitely shows the out-of-plane magnetization [Fig. 3(b)]. Comparing the morphology of 3.4 ML RT with that of 3.4 ML PA [see Figs. 1(b) and 1(e)], obviously nanostructuring (PA) of the thin film induces the out-of-plane magnetization. Figure 4(a) displays a series of XMCD spectra of PA as a function of Co coverage recorded in the $\mathbf{B}_{\perp}$ geometry. The out-of-plane magnetization is clearly observed in all PAs. Furthermore, it turns out that the magnitude of XMCD at the L_3 edge relative to the L_2 edge increases systematically with decreasing Co coverage.

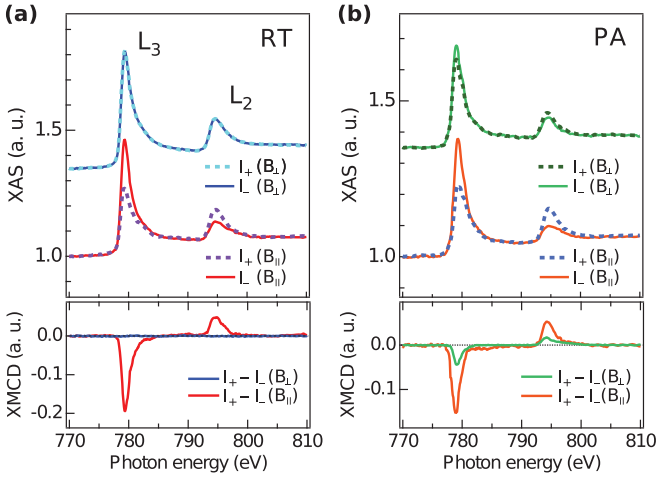

FIG. 3. (Color online) $L_{2,3}$ XAS and XMCD spectra of 3.4 ML (a) bcc Co thin film (RT) and (b) bcc Co nanostructures (PA) with the external magnetic field $\mathbf{B}$ of 1 T measured in the $\mathbf{B}_{\perp}$ and the $\mathbf{B}_{\parallel}$ geometries. The XAS spectra are normalized by the pre-edge intensity at 770 eV.

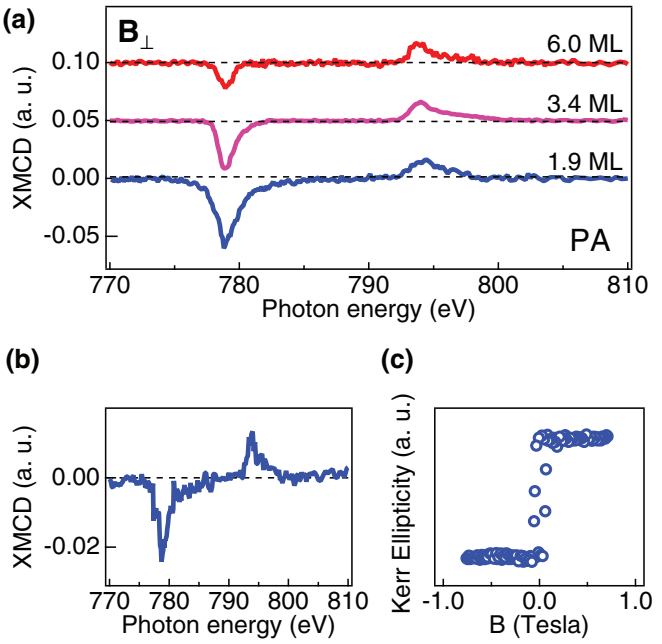

FIG. 4. (Color online) (a) XMCD spectra of bcc Co nanostructures (PA) as a function of Co coverage measured in the $\mathbf{B}_{\perp}$ geometry. The spectra are normalized to the L_2 intensity. (b) The out-of-plane remanent XMCD spectrum of 1.9-ML PA measured in the $\mathbf{B}_{\perp}$ geometry. (c) The in-plane easy axis hysteresis loop of 1.9-ML PA obtained by longitudinal Kerr effects measured at room temperature. The magnetic field is applied along the [110] direction of bcc Co.

An even more intriguing feature of PA is seen in the remanent magnetization. We have confirmed from the remanent $\mathbf{B}_\perp$ XMCD and longitudinal Kerr signals in Figs. 4(b) and 4(c) that 1.9 ML PA is ferromagnetic at room temperature and shows both (b) out-of-plane and (c) in-plane remanences. As for the origin of remanences, coalescences or interactions between islands are not probable. This is because reduced remanent $\mathbf{B}_\perp$ XMCD signal with increasing Co coverage is observed (not shown here), in contrast to the coalescence-induced ferromagnetism of the Co/Au(111) system [17]. In addition, the average distance between adjacent Co islands here is comparable to or greater than that of noninteracting Co islands on Au(788) [18]. Hence, these results provide a clear evidence of coexisting out-of-plane and in-plane remanences for the islands.

To elucidate the origin of coexisting remanences, the morphological dependence of the out-of-plane orbital ($L_\perp$) and spin ($S_\perp$) magnetic moments observed only in PA is examined by XMCD sum rules [19,20]. It should be noted, however, that evaluated magnetic moments of PA are lower limits since the highest available field of $\mathbf{B}_\perp = 1$ T may not be enough to guarantee full saturation of PA samples. The number of 2.22 for Co 3*d* holes, obtained from our *ab initio* calculation, is used here. We find that $L_\perp$ increases with decreasing Co coverage as shown by red squares in Fig. 5(a)

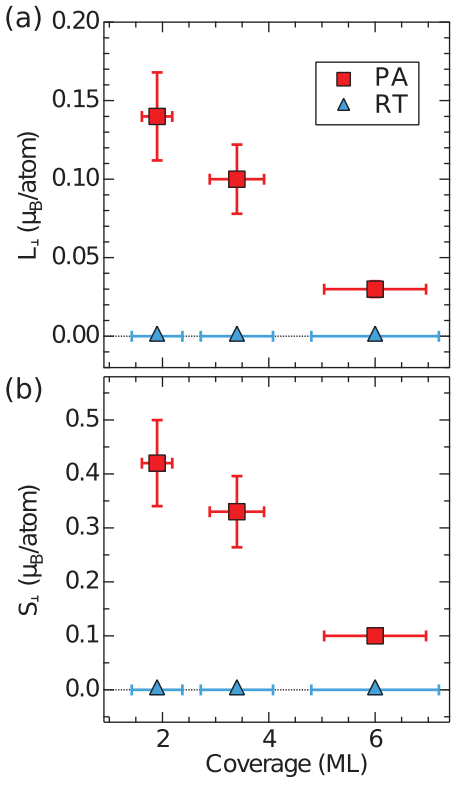

FIG. 5. (Color online) Out-of-plane orbital and spin magnetic moments, (a) $L_\perp$ and (b) $S_\perp$, of bcc Co nanostructures (PA: red squares) and thin films (RT: blue triangles) as a function of Co coverage. The horizontal error bars represent the deviations of the coverage determined by STM and the quartz crystal oscillator. The standard deviations of the estimated magnetic moments are shown by the vertical error bars.

(0.03 ± 0.01, 0.11 ± 0.01, and 0.14 ± 0.02 μ_B/atom for 6.0, 3.4, and 1.9 ML PA, respectively). This $L_\perp$ behavior is seen in other systems and can be related to the increased fraction of low coordinated atoms in the nanostructure [1,6]. Nanostructuring could enhance not only L but also S [4]. However, $S_\perp$ of PA, 0.10, 0.33, and 0.42 μ_B/atom for 6.0, 3.4, and 1.9 ML PA, respectively, shown by red squares in Fig. 5(b), is even smaller than the in-plane spin magnetic moment $S_\parallel$ of thick bcc Co films (1.44 μ_B/atom [14]).

C. Magnetic structure

To interpret such unexpectedly small $S_\perp$ values, first we assume genuine magnetic structures of PA based on the atomic coordination. The morphological dependence of $L_\perp$ in PA and the absence of $L_\perp$ and $S_\perp$ in RT (blue triangles in Fig. 5) indicate that the atomic sites with reduced coordination existing only in PA play the crucial role for the out-of-plane magnetization. Obviously, the rim atoms satisfy these conditions. On the other hand, core atoms would favor in-plane magnetization due to the similar atomic coordination as RT. Second, one has to take into account the exchange interaction, which favors a collinear spin alignment between rim and core atoms, to clarify the magnetic structures of PA.

Considering a relatively wide size distribution shown in Fig. 2(a), relatively larger islands, in which core atoms are dominant, favor the in-plane magnetization. However, as the size of the island decreases, rim atoms favoring out-of-plane magnetization become dominant and thus the rotation of the magnetization easy axis from the in-plane to the out-of-plane direction could occur. If such a nanostructure-size driven SRT occurs, coexisting remanences and apparently small $L_\perp$ and $S_\perp$ values obtained by XMCD are explainable since XMCD provides the average magnetic moments of the whole islands. This scenario is also applicable for PA at higher coverages. The less fractional population of rim atoms with increasing coverage results in lower $L_\perp$ and $S_\perp$ estimated by XMCD. It should be noted that the SRT proposed in this study is rather unusual. The SRT reported so far were mainly driven by the thickness and strains near the interface or surface of nanostructures [21]. The thickness of the capping layer was also an important factor to induce the SRT [22]. However, these factors are identical for the islands in this study.

Besides the nanostructure-size driven SRT, the out-of-plane magnetization observed by XMCD could be also low in the following cases: (1) partial rotation of Co moments caused by the external $\mathbf{B}_\perp$ field in such a case as the easy axis is toward in-plane directions or (2) a canted easy axis of magnetization. In the latter case, the magnetization direction of whole islands deviates from pure in-plane or out-of-plane directions and hence both $\mathbf{B}_\perp$ and $\mathbf{B}_\parallel$ XMCD signals could be detected.

However, these possibilities can be excluded as follows. As for case 1, the behaviors of $L_\perp$ and $S_\perp$ are inconsistent with the partial rotation. Such external-field-induced magnetization would be larger with increasing Co coverage since a smaller MAE is expected according to the quenching of the orbital moment due to stronger crystal field. This possibility is, however, definitely ruled out by our experimental results. In addition, the out-of-plane remanence should not be observed in this case, in contrast to our observation [Fig. 4(b)].

As for case 2, the easy magnetization direction of nanostructures is determined by the competition between the symmetry of the crystal structure (magnetocrystalline magnetic anisotropy) and morphology (shape magnetic anisotropy) and is normally toward pure in-plane or out-of-plane directions at the remanence [9]. When nanostructures are capped or supported by surfaces, the situation might change due to interfacial-strain-induced atomic relaxation, which could lead to the modification of the magnetization easy axis and MAE of nanostructures. Indeed, Nahas *et al.* demonstrated that the MAEs of Co nanodots on Au(111) changed drastically during Au encapsulation [23]. This is due to the change of atomic lattice parameters of the whole of the Co nanodots caused by the large lattice mismatch between Au(111) and hcp Co(111) (∼14% [24]). However, in the present study, the lattice mismatch between Au(001) including Au cap and bcc Co(001) is only ∼1.7% [10,12] and hence the atomic relaxation is negligible in both RT and PA. If the atomic relaxation is active, the modifications of the magnetization easy axis and MAE should be observed at least for the RT sample with the lowest coverage in this study (1.9 ML RT), where the influence from the Au substrate and Au cap is significant. The absence of the $\mathbf{B}_\perp$ XMCD signal of 1.9 ML RT is in contrast to this expectation. The canted easy axis can also be excluded experimentally by the XMCD-PEEM as explained in detail in the next paragraphs.

Eventually, we consider that the coexistence of in-plane and out-of-plane remanences of the islands is caused by the nanostructure-size driven SRT. Direct evidence of the SRT may be provided by the magnetic imaging of the islands with spin-polarized STM. However, this technique is not available in this study due to the presence of the Au surfactant layer on the islands. Instead, we have performed magnetic imaging with element specific XMCD-PEEM to confirm intrinsic in-plane magnetization of larger islands. With this technique, we can separately extract the magnetic information of bcc Co nanostructures from the Au surfactant layer and Au cap. In XMCD-PEEM, the remanent magnetization directions of domains are distinguishable from the azimuthal angular (Φ) dependence of the magnetization $\mathbf{M}$ while imaging domains as shown in Fig. 6(a). Since the XMCD intensity of magnetic domains is proportional to the projection of the magnetic moment $\mathbf{M}$ toward the direction of the incident x ray in XMCD-PEEM, a cosine (or sine) behavior as a function of Φ is expected for the in-plane magnetization (pink arrows) and constant behavior is expected for the out-of-plane magnetization (green arrows). In the case of the canted magnetization, $\mathbf{M}$ follows a cosine (or sine) behavior but does not show zero at the minimum.

Figure 6(b) shows an XMCD-PEEM image of 6.0 ML PA, which is suitable to investigate the magnetic properties of lager islands. Figure 6(c) shows the Φ dependence of $\mathbf{M}$ for the white contrast domains in the XMCD-PEEM image. The [110] direction is defined as $\Phi = 0^\circ$. $\mathbf{M}$ follows a cosine behavior with a positive maximum at 0° and zero at 90°, representing the magnetization direction along [110] (red arrow), which excludes the possibility of canted magnetization of PA. In the same way, magnetization directions of all the other domains are also found to be toward in-plane ⟨110⟩ directions (green and blue arrows), supporting that larger islands for 1.9 ML PA are in-plane magnetized. The evaluated in-plane orbital magnetic

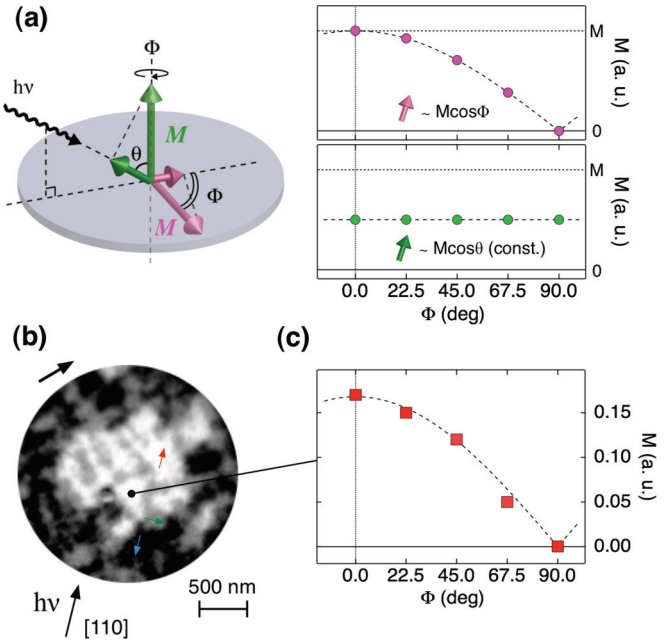

FIG. 6. (Color online) (a) Schematic explanation of the azimuthal angular (Φ) dependence of the magnetization $\mathbf{M}$. For in-plane magnetization, the projection of $\mathbf{M}$ follows a cosine function (M cos Φ) as shown by pink arrows. For out-of-plane magnetization, the projection is independent of Φ, providing a constant value (M cos θ) as shown by green arrows, where θ is the polar angle between the surface normal and the incident x ray. In this study, θ is set to 60°. (b) XMCD-PEEM domain image of 6.0 ML bcc Co nanostructure (PA), obtained by tuning the photon energy to the maximum of the Co L_3 absorption edge (∼778 eV). The direction of $h\nu$ is parallel to [110] of bcc Co at $\Phi = 0^\circ$. Local magnetization directions are shown by red, green, and blue arrows inside each domain. (c) The Φ dependence of $\mathbf{M}$ for white contrast domains. $\mathbf{M}$ is obtained by the intensity of the L_3 edge XMCD peak (∼778 eV) of the domains as a function of Φ. Each point is normalized by the pre-edge intensity at 775 eV. The sample is rotated from $\Phi = 0$ to 90° in steps of 22.5° in a clockwise direction.

moment ($L_\parallel$) of white contrast domains at $\Phi = 0^\circ$, namely, $0.27 \pm 0.02\ \mu_B$/atom, is in good agreement with $L_\parallel$ of 3.4 ML RT, $0.28 \pm 0.04\ \mu_B$/atom, derived from the XAS and XMCD spectra shown in Fig. 3(a). Comparable $L_\parallel$ values between 6.0 ML PA and 3.4 ML RT indicate that magnetic properties of PA become similar to those of RT as the nanostructure-size increases.

Thus, the XMCD-PEEM measurements for 6.0 ML PA reveal that magnetic domain walls exist between in-plane magnetized domains pointing in ⟨110⟩ directions. If a Bloch type domain wall separates these domains, a weak out-of-plane magnetization signal could be detected by the remanent $\mathbf{B}_\perp$ XMCD. Likewise, the out-of-plane magnetization induced by the Bloch wall would be also present for thicker RT (e.g., 3.4 ML RT) due to similar magnetic properties as 6.0 ML PA. Such behavior is not observed in the present results. Instead, possibly due to heterogeneity of thicker PA, we consider that there still exist smaller islands showing the out-of-plane magnetization, despite that most of their regions with larger domains are in-plane magnetized, which

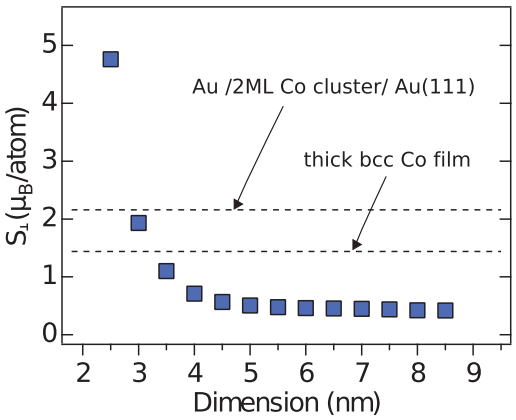

FIG. 7. (Color online) Out-of-plane spin magnetic moment of the smaller islands, $S_\perp^{\text{smaller}}$, in bcc Co islands (1.9 ML PA) as a function of the dimension of the island showing the out-plane-magnetization. The upper and lower dashed lines represent the spin magnetic moments of bilayer close packed Co clusters sandwiched between Au [17] and thick bcc Co films [14].

results in the emergence of the out-of-plane magnetization in XMCD. This is in line with the fact that we observed only in-plane magnetization and no out-of-plane magnetization in the XMCD-PEEM measurements since the spatial resolution of the experimental setup (∼20 nm) is not enough to detect the out-of-plane magnetization signals resulting from smaller islands.

D. Magnetic anisotropy

Room-temperature out-of-plane remanence shown in Fig. 4(b) caused by the smaller islands implies their large MAE. To evaluate the MAE of the smaller islands, we first extract a cutoff lateral island size of the smaller islands. Below this size, the islands are considered to be out-of-plane magnetized. The out-of-plane magnetic moments of the smaller islands can be extracted through the following equation of magnetic moments obtained by XMCD on the proposed nanostructure-size driven SRT model. Namely, $M_\perp^{\text{smaller}} f_{\text{smaller}} + M_\perp^{\text{larger}}(1 - f_{\text{smaller}}) = \text{M}_\perp$ ($M = L,S$), where $M_\perp^{\text{smaller}}$ ($M_\perp^{\text{larger}}$), $\text{M}_\perp$, and f_{smaller} denote the magnetic moments of the smaller (larger) islands, average magnetic moments, and fractional population of the islands below the cutoff lateral island size. Considering $L_\perp^{\text{larger}}$ ($S_\perp^{\text{larger}}$) ∼ 0 as manifested above, $L_\perp^{\text{smaller}}$ ($S_\perp^{\text{smaller}}$) is given by $L_\perp/f_{\text{smaller}}$ ($S_\perp/f_{\text{smaller}}$).

By virtue of the size distribution of the islands obtained by STM as shown in Fig. 2(a), we can directly evaluate f_{smaller} for each dimension. To find the most probable f_{smaller} value, we have plotted $S_\perp^{\text{smaller}}$ as a function of the dimension and compared it with the spin magnetic moment of bilayer close packed Co clusters sandwiched between Au [17] and that of thick bcc Co films [14]. The spin magnetic moment of nanostructures is a good candidate to determine the cutoff size (f_{smaller}) due to its nearly independent nature of the morphology and/or substrate [1,17]. $S_\perp^{\text{smaller}}$ obtained from $S_\perp = 0.42 \pm 0.06\ \mu_B$/atom for 1.9 ML PA shown in Fig. 5(b) and f_{smaller} as a function of the dimension is shown in Fig. 7. Note that $S_\perp^{\text{smaller}}$ would be larger than $S_\parallel$ of thick bcc Co films since nanostructuring enhances the spin magnetic moment due to the narrowing of the 3*d* band and an increase in the density of states near the Fermi level. Thus, it is found that only the cutoff size of about 3 nm ($f_{\text{smaller}} \sim 22\%$) gives a reasonable $S_\perp^{\text{smaller}}$ value for the nanostructure-size driven SRT. The extracted $S_\perp^{\text{smaller}}$ (∼ 1.9 μ_B/atom) [25] of the smaller islands shows a similar value as $S_\perp$ of close packed Co clusters [17].

Considering the room-temperature out-of-plane remanence, the perpendicular MAE per smaller island, $N\Delta E_{\text{SO}}$ (N: a number of Co atoms in the smaller island), must exceed the superparamagnetic limit of 645 meV (25 k_BT at 300 K) [26]. Rough estimation of ΔE_{SO} for typical smaller islands with a dimension of 3 nm ($N \sim 600$) leads to a large MAE of about 1.0 meV, which is considerably larger than the MAEs of close packed Co nanostructures or thin films [17,27].

The immediate question here is why is the MAE of the smaller islands large enough to show the room-temperature remanence? One reason is the vertical stacking of the smaller islands. The increased number of Co atoms enhances their ferromagnetic coupling energies compared to 1 ML height islands with the same lateral size. Another hint is given by a large difference in the blocking temperature T_b of the smaller islands embedded in Au (∼300 K) and T_b of close packed Co nanostructures on Pt(111) (∼100K) [8]. It is experimentally [2] and theoretically [28] well known that MAEs of 3*d* transition-metal systems increase by forming a 3*d*-5*d* interface with nonmagnetic 5*d* materials. As for the Co-Au system, Luis *et al.* demonstrated that the MAE of Co nanoparticles capped with Au was significantly enhanced, leading to an increase of T_b by a factor of 3 compared to the uncapped ones [29]. This is due to the strong SO coupling of Au atoms, which couple to surface Co atoms in Co nanoparticles via Co-Au hybridization. The smaller islands in this study are covered by Au, in contrast to vacuum in [8], and hence higher T_b can be expected.

The higher T_b is also plausible from the significant differences in the electronic band structures between bcc and close packed Co. A perturbation theory reveals that the 3*d* bandwidth W (exchange splitting Δ_{ex}) is inversely (directly) proportional to MAE. For bcc Co, W is approximately 1.5 eV narrower than that of close packed Co [30,31] and Δ_{ex} is the largest among 3*d* transition metals in accordance with the highest spin polarization [32]. Hence, the larger MAE of Co with the bcc phase compared with other phases is expected, resulting in higher T_b as well. Note that these two effects also enhance T_b of the larger islands, stabilizing the in-plane magnetization. As manifested above, such refinement of surrounding atoms and electronic band structures toward larger MAE in addition to the vertical stacking could establish the ferromagnetic order of bcc Co islands even at room temperature, leading to the coexistence of the out-of-plane and in-plane remanences.

IV. CONCLUSIONS

In conclusion, we have used XMCD to investigate magnetic properties of metastable bcc Co thin films and nanostructures on Au(001). While thin films show only the in-plane magnetization, the out-of-plane magnetization emerges additionally in nanostructures. Especially, the coexisting in-plane and out-of-plane remanences are confirmed for the islands. The

observed out-of-plane magnetization of nanostructures shows the coverage dependence as reported in other systems. Its magnitude is, however, unexpectedly smaller than the in-plane magnetization of thick films by a factor of more than 3. Combining these XMCD results with the results of the surface analysis technique by STM, consequently, we conclude that the nanostructure-size driven SRT of the magnetic easy axis from the in-plane to the out-of-plane direction with decreasing size is the most plausible interpretation to explain the coexisting in-plane and out-of-plane remanences for the islands. The validity of proposed SRT is reinforced by the intrinsic in-plane magnetization of the larger islands revealed by XMCD-PEEM. The out-of-plane remanence caused by the smaller islands with a large MAE of about 1 meV/atom is possibly attributed to (1) increased volume by the vertical stacking, (2) the effective interfacial effect between Co atoms in the smaller islands and surrounding Au atoms, and (3) the specific electronic band structure in the bcc Co phase.

ACKNOWLEDGMENTS

We thank M. Kotsugi, S. Itoda, S. Komori and Y. Nakatsu for technical assistance and scientific regarding the photoelectron emission microscope (PEEM) combined with x-ray magnetic circular dichroism (XMCD). The authors also thank Y. Suzuki for scientific advice regarding Kerr measurements. The XMCD and XMCD-PEEM experiments at BL25SU of SPring-8 were performed with the approval of the Japan Synchrotron Radiation Research Institute (Proposal No. 2007B1731). We gratefully acknowledge W. Wulfhekel for fruitful discussions. A part of the research was conducted under the financial support of a Grant in Aid for Japan Society for the Promotion of Science Fellows.

[1] P. Gambardella, S. Rusponi, M. Veronese, S. S. Dhesi, C. Grazioli, A. Dallmeyer, I. Cabria, R. Zeller, P. H. Dederichs, K. Kern, C. Carbone, and H. Brune, Science **300**, 1130 (2003).

[2] J. Bartolomé, L. M. García, F. Bartolomé, F. Luis, R. López-Ruiz, F. Petroff, C. Deranlot, F. Wilhelm, A. Rogalev, P. Bencok, N. B. Brookes, L. Ruiz, and J. M. González-Calbet, Phys. Rev. B **77**, 184420 (2008).

[3] J. Stöhr, J. Magn. Magn. Mater. **200**, 470 (1999).

[4] P. Gambardella, A. Dallmeyer, K. Maiti, M. C. Malagoli, W. Eberhardt, K. Kern, and C. Carbone, Nature (London) **416**, 301 (2002).

[5] P. Bruno, Phys. Rev. B **39**, 865(R) (1989).

[6] H. A. Dürr, S. S. Dhesi, E. Dudzik, D. Knabben, G. van der Laan, J. B. Goedkoop, and F. U. Hillebrecht, Phys. Rev. B **59**, R701 (1999).

[7] P. Ohresser, N. B. Brookes, S. Padovani, F. Scheurer, and H. Bulou, Phys. Rev. B **64**, 104429 (2001).

[8] S. Rusponi, T. Cren, N. Weiss, M. Epple, P. Buluschek, L. Claude, and H. Brune, Nature Mater. **2**, 546 (2003).

[9] S. Chikazumi, *Physics of Ferromagnetism* (Oxford University Press, New York, 1997).

[10] T. Kawagoe, T. Miyamachi, M. Someta, T. Kudo, and S. Suga, Surf. Sci. **602**, L15 (2008).

[11] Y. Saitoh, H. Kimura, Y. Suzuki, T. Nakatani, T. Matsushita, T. Muro, T. Miyahara, M. Fujisawa, K. Soda, S. Ueda, H. Harada, M. Kotsugi, A. Sekiyama, and S. Suga, Rev. Sci. Instrum **71**, 3254 (2000).

[12] N. Spiridis, T. Ślęzak, M. Zajac, and J. Korecki, Surf. Sci. **566**, 272 (2004).

[13] L. Z. Mezey and J. Giber, Jpn. J. Appl. Phys. **21**, 1569 (1982).

[14] P. Ryan, R. P. Winarski, D. J. Keavney, J. W. Freeland, R. A. Rosenberg, S. Park, and C. M. Falco, Phys. Rev. B **69**, 054416 (2004).

[15] Y. Z. Wu, H. F. Ding, C. Jing, D. Wu, G. L. Liu, V. Gordon, G. S. Dong, X. F. Jin, S. Zhu, and K. Sun, Phys. Rev. B **57**, 11935 (1998).

[16] X. Liu, R. L. Stamps, R. Sooryakumar, and G. A. Prinz, Phys. Rev. B **54**, 11903 (1996).

[17] T. Koide, H. Miyauchi, J. Okamoto, T. Shidara, A. Fujimori, H. Fukutani, K. Amemiya, H. Takeshita, S. Yuasa, T. Katayama, and Y. Suzuki, Phys. Rev. Lett. **87**, 257201 (2001).

[18] N. Weiss, T. Cren, M. Epple, S. Rusponi, G. Baudot, S. Rohart, A. Tejeda, V. Repain, S. Rousset, P. Ohresser, F. Scheurer, P. Bencok, and H. Brune, Phys. Rev. Lett. **95**, 157204 (2005).

[19] C. T. Chen, Y. U. Idzerda, H.-J. Lin, N. V. Smith, G. Meigs, E. Chaban, G. H. Ho, E. Pellegrin, and F. Sette, Phys. Rev. Lett. **75**, 152 (1995).

[20] B. T. Thole, P. Carra, F. Sette, and G. van der Laan, Phys. Rev. Lett. **68**, 1943 (1992).

[21] F. El Gabaly, S. Gallego, C. Muñoz, L. Szunyogh, P. Weinberger, C. Klein, A. K. Schmid, K. F. McCarty, and J. de la Figuera, Phys. Rev. Lett. **96**, 147202 (2006).

[22] H. W. Zhao, Y. Z. Wu, C. Won, F. Toyoma, and Z. Q. Qiu, Phys. Rev. B **66**, 104402 (2002).

[23] Y. Nahas, V. Repain, C. Chacon, Y. Girard, J. Lagoute, G. Rodary, J. Klein, S. Rousset, H. Bulou, and C. Goyhenex, Phys. Rev. Lett. **103**, 067202 (2009).

[24] B. Voigtländer, G. Meyer, and N. M. Amer, Phys. Rev. B **44**, 10354 (1991).

[25] Note that $S_{\perp}^{\text{smaller}}$ contains 7 $m_T^{\perp}$, where $m_T^{\perp}$ denotes the out-of-plane magnetic dipole term. It is reported that the direction of $m_T^{\perp}$ is the same as that of the spin magnetic moment and the absolute value of 7 $m_T^{\perp}$ is between 0.2 and 0.3 μ_B/atom for Co clusters or thin films. Hence, the values of $S_{\perp}^{\text{smaller}}$ shown in Fig. 7 could be overestimated compared to the intrinsic spin magnetic moment.

[26] O. Fruchart, M. Klaua, J. Barthel, and J. Kirschner, Phys. Rev. Lett. **83**, 2769 (1999).

[27] D. Weller, J. Stöhr, R. Nakajima, A. Carl, M. G. Samant, C. Chappert, R. Mégy, P. Beauvillain, P. Veillet, and G. A. Held, Phys. Rev. Lett. **75**, 3752 (1995).

[28] Y. Xie and J. A. Blackman, Phys. Rev. B **74**, 054401 (2006).

[29] F. Luis, J. Bartolomé, F. Bartolomé, M. J. Martínez, L. M. García, F. Petroff, C. Deranlot, F. Wilhelm, and A. Rogalev, J. Appl. Phys. **99**, 08G705 (2006).

[30] G. A. Prinz, E. Kisker, K. B. Hathaway, K. Schröder, and K. H. Walker, J. Appl. Phys. **57**, 3024 (1985).

[31] D. A. Papaconstantopoulos, *Handbook of the Band Structure of Elemental Solids* (Plenum, New York, 1986).

[32] S. Yuasa, A. Fukushima, H. Kubota, Y. Suzuki, and K. Ando, Appl. Phys. Lett. **89**, 042505 (2006).